ELSEVIER

Contents lists available at ScienceDirect

# International Journal of Heat and Mass Transfer

journal homepage: www.elsevier.com/locate/hmt



# Dual-function thermoelastic cloak based on coordinate transformation theory



Yu-Ze Tian<sup>a</sup>, Yan-Feng Wang<sup>a,\*</sup>, Gan-Yun Huang<sup>a,\*</sup>, Vincent Laude<sup>b</sup>, Yue-Sheng Wang<sup>a,c</sup>

- <sup>a</sup> School of Mechanical Engineering, Tianjin University, Tianjin 300350, China
- <sup>b</sup> Institut FEMTO-ST, Univ. Bourgogne Franche-Comté, CNRS, Besançon, France
- <sup>c</sup> Institute of Engineering Mechanics, Beijing Jiaotong University, Beijing 100044, China

#### ARTICLE INFO

Article history: Received 19 February 2022 Revised 23 April 2022 Accepted 8 June 2022

Keywords: Cloak Thermoelasticity Coordinate transformation Metamaterials

#### ABSTRACT

In past years, various cloaks have attracted the attention of many scientists but they usually remain confined to a single function. Cloaks combining multiple functions, however, are desirable. In this paper, we design thermoelastic cloaks with dual functionality by the coordinate transformation technique. The transformation of the thermoelastic wave equations for cloaking and explicit expressions for the required material parameters are established. Symmetrization of the elastic tensor is applied using Norris' gauge matrix to emphasize the feasibility of the designs. Two different operating conditions, transient elastic wave propagation and steady heat transfer, are adopted in numerical calculations for the designed cloaks. It is shown that, on one hand, from the perspective of observer, whether the cloak is symmetrized or not, its external response is identical and invisibility is reliable. On the other hand, it is destined that the symmetrization of the cloak would be accompanied by the increase of internal displacement, which may need to be paid attention to in the actual design. In addition, the temperature effects of both cloaks are consistent. The work in this paper may pave a way toward the realization of thermoelastic cloaks, thus broadening the research scope for metamaterials.

© 2022 Elsevier Ltd. All rights reserved.

#### 1. Introduction

Since the concept of metamaterials was proposed, a large number of devices with abnormal properties have been designed [1]. As a popular application, the invisibility of objects has been widely discussed in different physical fields. Theories including wavefront regulation based on the generalized Snell's law [2] and active cloaks based on scattering extinction [3,4] have been widely reported. Among them, the transformation cloak has achieved wide recognition due to its flexibility and adaptability to various conditions. This type of cloak is brought out by expressing coordinate transformation invariance. Owing to the simultaneous achievement of invariance in different governing equations, objects may be made simultaneously invisible to multiphysical incident fields.

Transformation invariance was first found by Greenleaf through analysis of Maxwell's equations [5]. Building on this idea, Pendry et al. [6] and Leonhardt [7] both proposed an electromagnetic transformation cloak. A protected vacuum space would be created in the surrounding electromagnetic field, where internal ob-

E-mail addresses: wangyanfeng@tju.edu.cn (Y.-F. Wang), gyhuang@tju.edu.cn (G.-Y. Huang).

jects could not be perceived externally and thus would remain hidden. Using the analogy between transverse-electric electromagnetic waves and acoustic waves in inviscid fluids, a 2D acoustic cloak was further designed by Cummer [8]. After that, Chen et al. [9] extended the result to the 3D case and a series solution for acoustic waves was given. Considering the symmetry of the biharmonic equation, a layered transformation cloak for thin plates was designed by Farhat et al. [10] with the help of effective medium theory. For a rigorous physical interpretation, Zareei et al. [11] discussed the correlation between the transformed flexural wave equation and the anisotropic plate model. Recently, Golgoon et al. [12] established a compatibility equation giving a comprehensive explanation of bending wave invisibility. On the experimental side, cloaks for electromagnetic waves [13], acoustic waves [14] and bending waves have been successfully demonstrated [15]. These results suggest a wider application of effective media theory. Based on transformation theory, cloaks have been extensively developed as well for heat flows [16], diffusion [17], water waves [18], and matter waves [19].

A difficulty is that transformation theory is not directly applicable to the Lamé-Navier equations describing elastic waves in general. The coupling of longitudinal and transverse waves makes the manipulation even more difficult. Milton et al. [20] provided

<sup>\*</sup> Corresponding author.

an improvement for the coordinate transformation of the elasto-dynamic equation. The transformed elastic constitutive relations are highly consistent with the Willis equations proposed in 1981 [21]. Acknowledging this fact, the designed cloak is known as a Willis-cloak. Discarding the symmetry of the elastic tensor, the transformation was further simplified by Brun et al. [22]. Nassar et al.[23] gave a solution to asymmetric constitutive relation with degenerate polar lattice. Then, based on microcontinuum theory, a static cloak has been successfully demonstrated experimentally with Cosserat materials by Xu et al[24]. Subsequently, Norris et al. [25] summarized these two types of cloaks and established a common framework. Interestingly, the above designs can be simplified if mixed modes can be separated. The proposal of pentamode metamaterials made this concept possible [26] and also provided a new pathway for the design of acoustic metasurfaces [27–29].

Since different physical fields are often associated in practice, cloaks with a single function may not provide the expected invisibility. For example, electricity and heat flows, and traveling stresses always coexist in computing devices. Temperature rise and unevenly distributed stress on the substrate are often the main reasons of damage. In the field of high-speed PCBs [30] or chips [31], heat concentration [32,33] and the excitation of elastic waves [34,35] have attracted much attention. Syvret et al. [36] analyzed the possible breaking of thermal invisibility caused by coupling effect, illustrating the shortcomings of existing single function cloaks in a coupled field.

With such issues of multiphysics coupling, metamaterial coat [37,38] became one of the solutions favored in recent years. It is not only ultrathin, but also undetectable in a broad frequency range together with the objects. Due to the high degree of freedom, topology optimization has been applied to the structural design of multiphysics cloaks. The designed cloaks could manipulate the heat flux and direct a current [60], or work for both electromagnetic waves and sound waves of different wavelengths [39]. Nonetheless, it seems that transformation theory is seldom reported in multiphysical metamaterials. Li et al. [40] proposed a design for a dual-function cloak via transformation to achieve the simultaneous regulation of heat flow and electric field. This design was further extended by Ma et al. [41]. The physical coupling effect, however, was still not considered together with transformation theory yet. A new strategy was then given by Stedman [42] et al considering the Seebeck effect. Their treatment of coupling terms provided this theory with new possibilities for multiphysical invisibility. In the case of thermo-mechanical coupling, an elastostatic cloak under thermal gradients was designed by Alvarez et al. [43] with the help of optimization. It can ensure the independent response of the background and the central hole. However, cloak protection and invisibility in the temperature field are not achieved. The design of dual-function thermoelastic cloaks including physical coupling effects thus still needs further exploration.

In this paper, we develop transformation theory under the framework of thermoelasticity. The transformed thermoelastic equations, based on Biot's thermoelasticity theory [44], are derived. Symmetrization of the transformed elastic tensor by application of a gauge matrix and the correct setting of boundary conditions is discussed. Both transformed thermoelastic equations are verified by numerical evaluation of the resulting cloaks. Their invisibility and isolation capabilities are compared. It is expected that this work can lay a theoretical foundation for transformation thermoelasticity.

### 2. Transformation theory

The original space and the transformed space are denoted by  $\Pi$  and  $\pi$ , respectively. Particles in corresponding spaces are described by vectors  $X_l$  and  $x_i$ , between which a point-wise mapping  $\mathcal{F}$  is

determined. The transformation matrix is defined as  $F_{il} = \partial x_i/\partial X_l$ . The uppercase and lowercase subscript correspond to the factors in two spaces respectively. Furthermore, Norris' gauge matrix  $A_{ij}$  [25] is introduced:

$$U_I = A_{iI} U_i^{\prime} \tag{1}$$

where  $U_l$  and  $U_i^{'}$  correspond to the displacement vector fields in spaces  $\Pi$  and  $\pi$ , respectively. The summation convention on repeated subscripts is assumed.

# 2.1. Transformation thermoelasticity theory

In any subspaces  $\Omega \subseteq \Pi$  the thermoelastic dynamical equations in the absence of source read:

$$\left(C_{IJKL}U_{L,K} + \beta_{IJ}\Delta T\right)_{,J} = \rho \ddot{U}_{J},\tag{2}$$

$$\left(\kappa_{JL}T_{,L}\right)_{,I} = C_{V}\dot{T} + T_{0}\beta_{KL}\dot{U}_{L,K},\tag{3}$$

where  $C_{IJKL}$  is a fourth-order elasticity tensor satisfying the full symmetry:

$$C_{IJKL} = C_{IIKL} = C_{IJLK}, \quad C_{IJKL} = C_{KLIJ}. \tag{4}$$

 $\rho$  is the isotropic scalar mass density and  $C_V$  is the volumetric heat scalar capacity of the background medium carrying conventional properties.  $\beta_{IJ}$  and  $\kappa_{KL}$  are the second-order thermal expansion tensor and thermal conductivity tensor, respectively. Anisotropy of these two tensors is allowed and their symmetry is generally guaranteed.  $\Delta T$  represents the local variation of temperature.  $\dot{T}$  and  $\dot{U}_I$  represent the first-order time derivative of temperature and displacement (i.e. velocity vector) respectively, and  $\ddot{U}_I$  represents the second-order time derivative of displacement (i.e. acceleration vector).

For simplicity, the boundary  $\partial\Omega$  is set to satisfy the Neumann condition for both physical fields:

$$n_I \left( C_{IJKL} U_{L,K} + \beta_{IJ} \Delta T \right) dS \Big|_{\partial \Omega} = P_J dS \Big|_{\partial \Omega},$$
 (5)

$$n_J(\kappa_{JL}T_{,L})dS\big|_{\partial\Omega} = QdS\big|_{\partial\Omega},$$
 (6)

where  $P_J = P_J(X_I,t)$  and  $Q = Q(X_I,t)$  indicate the external loading of force and heat flow, respectively. The load here can be arbitrary or set to Dirichlet conditions of prescribed displacement and temperature, which would actually have no effect on the subsequent conclusions. The key point here is that the flux conservation relations on the boundary of selected internal regions must remain after transformation. Under the framework of thermoelasticity, these flux relations should be physically interpreted as the continuity of traction and normal heat flow. We further define the stress tensor by  $s_{IJ} = C_{IJKL}U_{L,K} + \beta_{IJ}\Delta T$  and the heat flux vector by  $q_J = \kappa_{JL}T_{.L}$ . Therefore these continuities on the boundary of an arbitrary subdomain  $M \subseteq \Omega$  are expressed as:

$$n_I s_{IJ} dS \big|_{\partial M, \text{in}} = n_I s_{IJ} dS \big|_{\partial M, \text{out}},$$
 (7)

$$n_J q_J dS \big|_{\partial M, \text{in}} = n_J q_J dS \big|_{\partial M, \text{out}},$$
 (8)

where the subscripts in and out are used to distinguish the inside and the outside of the boundary, as shown in Fig. 1(a).

A subdomain  $m \subseteq \pi$  can be obtained by application of the mapping  $m = \mathcal{F}(M)$ . In general, the spatial topology of m is only determined by the mapping  $\mathcal{F}: M \to m$ . In this paper, its outer boundary is set to be attached to the outside of  $\partial M$  as shown in Fig. 1(b). Such a configuration ensures that the background field is not affected by the coordinate transform.

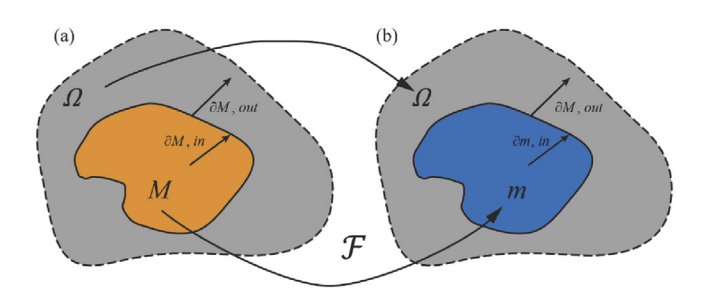


Fig. 1. Spatial configuration (a) before and (b) after coordinate transformation.

First, the continuity on the boundary  $\partial m$  needs to be guaranteed. Using the chain rule and Nanson's formula on Eqs. (7) and (8), the flux relationship under the coordinate transformation should be set as:

$$n_{i}^{\prime}J^{-1}F_{iI}\left(C_{IJKL}U_{L,K}F_{kK} + \beta_{IJ}\Delta T\right)dS\Big|_{\partial m, \text{in}} = n_{I}s_{IJ}dS\Big|_{\partial M, \text{out}}, \tag{9}$$

$$n'_{j}J^{-1}F_{jJ}(\kappa_{JL}T_{,l}F_{lL})dS\big|_{\partial m.\text{in}} = n_{J}q_{J}dS\big|_{\partial M.\text{out}},$$
(10)

where  $J \triangleq \det(F)$  is the Jacobian determinant of matrix F. Considering the transformed parameters:

$$C'_{ijkL} = J^{-1}F_{il}F_{kK}C_{ljKL}, \tag{11}$$

$$\beta_{iJ}' = J^{-1} F_{iJ} \beta_{IJ}, \tag{12}$$

$$\kappa_{il}' = J^{-1} F_{iJ} F_{lL} \kappa_{JL}, \tag{13}$$

$$\rho' = J^{-1}\rho,\tag{14}$$

$$C_{v}' = I^{-1}C_{V},$$
 (15)

and transformed variables:

$$U_i' = U_i, \tag{16}$$

$$T' = T, (17)$$

the flux relationship Eqs. (9) and (10) can be expressed as:

$$n_i' \left( C_{iJkL}' U_{L,k}' + \beta_{iJ}' \Delta T' \right) dS \Big|_{\partial m.\text{in}} = n_I s_{IJ} dS \Big|_{\partial M.\text{out}}, \tag{18}$$

$$n_{j}'(\kappa_{jl}'T_{l}')dS|_{\partial m \text{ in}} = n_{j}q_{j}dS|_{\partial M \text{ out}}, \tag{19}$$

while the governing equation in m under the transformed coordinate can be also obtained:

$$\left(C'_{ilkl}U'_{l,k} + \beta'_{il}\Delta T'\right)_{i} = \rho'\ddot{U}'_{l},\tag{20}$$

$$\left(\kappa_{il}^{\prime}T_{,l}^{\prime}\right)_{i} = C_{v}^{\prime}\dot{T}^{\prime} + T_{0}\beta_{kl}^{\prime}\dot{U}_{L,k}^{\prime}.\tag{21}$$

The transformed boundary conditions Eqs. (18) and (19) can be noted to have the same form as Eqs. (7) and (8), while the transformed governing equations (20) and (21) have the same form as Eqs. (2) and (3), too. This form invariance of both continuity and governing equations makes it possible to interpret physically each term in the transformed equations. In particular, the transformed thermoelastic constitutive relation reads:

$$\sigma_{il}' = C_{ilkl}' U_{l,k}' + \beta_{il}' \Delta T'. \tag{22}$$

If matrix F is not symmetric, then the asymmetry of the elastic tensor and of the thermal stress tensor results from the absence of minor symmetries:

$$C'_{ijkL} \neq C'_{jikL}, \quad C'_{ijkL} \neq C'_{ijLk}, \quad \beta'_{ij} \neq \beta'_{Ji}.$$
 (23)

To give an explicit physical interpretation, we define:

$$C_{iJkL}^{\prime E} = \frac{1}{2} \left( C_{iJkL}^{\prime} + C_{iJLk}^{\prime} \right), \tag{24}$$

$$D_{ijkL}^{\prime E} = \frac{1}{2} \left( C_{ijkL}^{\prime} - C_{ijLk}^{\prime} \right), \tag{25}$$

$$\omega_{kL}' = \frac{1}{2} \left( \frac{\partial U_k'}{\partial x_I'} - \frac{\partial U_L'}{\partial x_\nu'} \right), \tag{26}$$

$$\beta_{il}^{\prime} \Delta T^{\prime} = C_{ilkl}^{\prime E} \alpha_{kl}^{\prime E} \Delta T^{\prime} + D_{ilkl}^{\prime E} \alpha_{kl}^{\prime \omega} \Delta T^{\prime}. \tag{27}$$

Furthermore Eq. (22) can be written:

$$\sigma_{il}' = C_{ilkL}'^{E} \left( \varepsilon_{kL}'^{E} + \alpha_{kL}'^{E} \Delta T' \right) + D_{ilkL}'^{E} \left( \omega_{kL}'^{E} + \alpha_{kL}'^{\omega} \Delta T' \right). \tag{28}$$

 $\omega_{kL}^{\prime E}$  is the antisymmetric rotation tensor. The two thermal related tensors  $\alpha_{kL}^{\prime E}$  and  $\alpha_{kL}^{\prime \omega}$  are the strain tensor and the rotation tensor per unit temperature, respectively. The former is obviously consistent with the linear thermal expansion tensor, the anisotropy of which is thus allowed, while the latter is a case covered in [45]. In the case that the stress  $\sigma_{ij}^{\prime}$  is asymmetric, the couple stress should be introduced:

$$m'_{il} = B'^{E}_{ilkL} \left( \varepsilon^{\prime E}_{kL} + \alpha^{\prime \varepsilon}_{kL} \Delta T' \right) + A'^{E}_{ilkL} \left( \omega^{E}_{kL} + \alpha^{\prime \omega}_{kL} \Delta T' \right), \tag{29}$$

where  $B_{ijkL}^{\prime E} = D_{klji}^{\prime E}$ . The constitutive relation given by Eqs. (28) and (29) is known as micropolar theory [46]. One can program these material parameters by artificially designing chiral non-centrosymmetric unit cells [47].

Eqs. (20) and (21) have similarities with Eqs. (68) and (69) given in Ref. [ [36]]. This does not imply the commonality of coordinate transformation theory and incremental theory, however, as both theories have obvious different physical meanings. Transformation theory is built upon the mapping between different spaces  $\Pi$  and  $\pi$  from which one obtains the material parameter distribution that is required to achieve a desired function. Incremental theory builds a transformation between two different reference configurations of the same physical body, with the aim of solving problems in a unified form.

By adjusting the mapping  $\mathcal{F}$ , different material parameter distributions can be obtained [48]. The subdomain m would be designed as a wave-steering device with different functions, such as a rotator, a lens or an invisibility cloak. The invisibility cloak may be considered a special case as one or more holes need to be introduced in the domain represented in Fig. 1(b). Such changes in topology lead to singularities, inevitably.

When thermoelastic coupling is negligible, the above configurations will degenerate into a decoupled Cosserat-type transformation elastic cloak and a decoupled transformation heat cloak:

$$\left(C'_{ijkL}U'_{L,k}\right)_{i} = \rho'\ddot{U}'_{J}, \qquad \text{in } m, \tag{30}$$

$$\left(\kappa'_{jl}T'_{,l}\right)_{,j} = C'_{V}\dot{T}', \qquad \text{in } m, \tag{31}$$

with boundary conditions:

$$n_i'C_{iJkL}'U_{L,k}'dS\big|_{\partial m.in} = n_lC_{IJKL}U_{L,K}dS\big|_{\partial M.out},$$
 (32)

$$n'_{j}\kappa'_{jl}T'_{,l}dS\big|_{\partial m \text{ in}} = n_{J}\kappa_{JL}T_{,L}dS\big|_{\partial M \text{ out}}.$$
(33)

#### 2.2. Symmetrized transformation thermoelasticity theory

The asymmetric constitutive relations defined by Eqs. (28) and (29) may be achieved by materials containing chiral structures, though its artificial design in this case is always limited by noncentrosymmetry [47]. However, there are many reports on the artificially designed arbitrary symmetric elastic constitutive relations [49–55] and thermal expansion tensors [56–58]. Thus, one may hope to seek an approach to make material tensors defining the devices symmetrical, at the same time retaining the performance of the design to a permissible level.

Technically, the remaining two capital subscripts in space  $\Pi$  in Eq. (20) need to be transformed into space  $\pi$  to ensure the symmetry of subscript pairs (i,j) and (k,l). In this section, the gauge transformation defined by Eq. (1) is introduced, similar to Milton et al [20] and Norris et al [25], to test the mechanism of this method under the framework of transformation thermoelastic. We select  $A_{il} = F_{il}$  in order to symmetrize the elastic and thermal expansion tensors, which leads to new governing equations. To distinguish notations from the previous section,  $U_i^{''}$  is used here to represent the displacement after gauge transformation (the domain here is named differently m'):

$$\left[J^{-1}F_{il}C_{IJKL}F_{kK}\left(A_{IL}U_{l}^{\prime\prime}\right)_{,k}+J^{-1}F_{il}\beta_{IJ}\Delta T\right]_{,i}=$$

$$J^{-1}\rho\left(A_{iJ}\ddot{U}_{l}^{\prime\prime}\right), \quad \text{in } m^{\prime}, \tag{34}$$

$$\left[ J^{-1} F_{iI} \left( \kappa_{IJ} F_{jJ} T_{,j} \right) \right]_{i} = J^{-1} C_{V} \dot{T} + J^{-1} F_{iI} \beta_{IJ} \left( A_{jJ} U_{j}^{"} \right)_{,i},$$
in  $m'$ ,
(35)

with boundary conditions:

$$n'_{i}J^{-1}F_{il}\left(C_{IJKL}F_{kK}\left(A_{IL}U_{l}^{\prime\prime}\right)_{,k}+\beta_{IJ}\Delta T\right)dS\Big|_{\partial m',\text{in}}=$$

$$n_{l}S_{IJ}dS\Big|_{\partial M,\text{OUT}},$$
(36)

$$n_{i}^{\prime}J^{-1}F_{il}(\kappa_{IJ}F_{jJ}T_{,j})dS|_{\partial m^{\prime}\text{ in}} = n_{I}q_{I}dS|_{\partial M.\text{Out}},$$
(37)

and implicit continuity conditions:

$$A_{il}U_i''\big|_{\partial m', \text{in}} = U_I|_{\partial M, \text{out}},\tag{38}$$

After these processes, the physical meaning of the terms in Eq. (34) is still unclear. The mass density is effectively not only anisotropic but also asymmetric. The coupling terms in Eqs. (34) and (35) do not match as well. Gauge freedom can be invoked again: gauge matrix  $A_{il}$  can be multiplied with the free index I on both sides of Eq. (34). Mathematically, it means only considering a linear combination of the system of equations, which is equivalent to the initial system of equation if A is non singular. For the same reason, boundary condition Eq. (36) is preserved. The distribution of displacement would not be changed due to the uniqueness of the solution of the wave equation:

$$A_{JJ} \left[ J^{-1} F_{iI} C_{IJKL} F_{kK} \left( A_{IL} U_I'' \right)_{,k} + J^{-1} F_{IJ} \beta_{IJ} \Delta T \right]_{,i} =$$

$$J^{-1} A_{JJ} \rho \left( A_{IJ} \ddot{U}_{i}'' \right), \text{ in } m'.$$
(39)

Because the gauge matrix only rearranges the distribution of the displacement  $U_i$  inside subdomain m, the external environment is not influenced, and the same solution as in Eq. (20) can be obtained. Still, it is difficult to explain the physical meaning of the equation clearly. Using the identity:

$$(P_{ij}Q_{jk})_{i} = (P_{ij})_{i}Q_{jk} + P_{ij}(Q_{jk})_{i},$$
 (40)

Eq. (39) can be transformed into a new governing equation:

$$\left(C_{ijkl}^{"}U_{l,k}^{"}+S_{ijl}^{"}U_{l}^{"}+\beta_{ij}^{"}\Delta T\right)_{i}=$$

$$\rho_{ii}''\ddot{U}_{i}'' + D_{ikl}''U_{k,l}'' + E_{il}''U_{l}'' + \gamma_{i}''\Delta T, \quad \text{in } m', \tag{41}$$

with:

$$C_{ijkl}^{"} = J^{-1}F_{il}A_{il}F_{kK}A_{lL}C_{llKL}, (42)$$

$$S_{iil}^{"} = J^{-1} F_{il} A_{jl} A_{lL,K} C_{lJKL}, \tag{43}$$

$$D_{ikl}^{"} = J^{-1}A_{jl,l}F_{kK}A_{lL}C_{lJKL}, (44)$$

$$E_{jl}'' = J^{-1}A_{jJ,l}A_{lL,K}C_{lJKL}, (45)$$

$$\rho_{ij}^{"} = J^{-1} A_{il} A_{jl} \rho, \tag{46}$$

$$\beta_{ii}^{"} = J^{-1} F_{il} A_{jl} \beta_{lj}, \tag{47}$$

$$\gamma_i'' = J^{-1} A_{jJ,I} \beta_{IJ}. \tag{48}$$

Due to the limitation of Eq. (38), the degradation condition needs to be introduced on the boundary:

$$A_{il}|_{\partial m', \text{in}} = I_{il}|_{\partial m', \text{in}}.$$
(49)

where  $l_{il}$  is the identity matrix. Therefore a more general continuity condition can be obtained:

$$U_l''\big|_{\partial m', \text{in}} = U_l\big|_{\partial M, \text{out}}.$$
 (50)

with the stress equilibrium boundary condition:

$$n'_{i} \left( C''_{ijkl} U''_{l,k} + S''_{ijl} U''_{l} + \beta''_{ij} \Delta T \right) dS \Big|_{\partial m', \mathbf{in}} =$$

$$n_{l} s_{lj} dS \Big|_{\partial M, \mathbf{out}}.$$

$$(51)$$

Since the gauge matrix is only a local transformation of the dependent variable, the normal vector  $n_i'$  in Eq. (51) would not be changed. The adjustment from Eqs. (39) to (41) does accompany the change of flux/stress relationship, but the displacement field  $U_i''$  is not affected. One can choose an arbitrary subdomain  $\Phi$  within m', on whose boundary  $\partial \Phi$  the flux condition derived from Eq. (39) reads:

$$n_{i}^{\prime}J^{-1}F_{il}\left(C_{IJKL}F_{kK}\left(A_{IL}U_{l}^{\prime\prime}\right)_{,k}+\beta_{IJ}\Delta T\right)dS\Big|_{\partial\Phi,\text{in}}=$$

$$n_{i}^{\prime}J^{-1}F_{il}\left(C_{IJKL}F_{kK}\left(A_{IL}U_{l}^{\prime\prime}\right)_{,k}+\beta_{IJ}\Delta T\right)dS\Big|_{\partial\Phi,\text{OUT}},$$
(52)

while the one derived from Eq. (41) reads:

$$n'_{i}\left(C''_{ijkl}U''_{l,k} + S''_{ijl}U''_{l} + \beta''_{ij}\Delta T\right)dS\Big|_{\partial\Phi, \mathbf{in}} = n'_{i}\left(C''_{ijkl}U''_{l,k} + S''_{ijl}U''_{l} + \beta''_{ij}\Delta T\right)dS\Big|_{\partial\Phi, \mathbf{out}}.$$

$$(53)$$

Eqs. (52) and (53) are the specific expressions of Cauchy formula with different definitions of stress given by Eqs. (39) and (41), respectively. It is obvious that they are inconsistent in physical meaning. After multiplying both ends of Eq. (52) by  $A_{jj}$ , it would be noticed that the two actually have the same constraint on  $U_i''$ . In addition, considering the degradation condition Eq. (49), Eq. (36) is equivalent to Eq. (50) on  $\partial m'$ . Therefore, the conclusion can be drawn that the above process would not make any differences to the performance of our target.

Then, we represent the temperature in heat-conduction Eqs. (21) under transformed coordinates:

$$T'' = T, (54)$$

with the parameters:

$$\kappa_{il}^{"} = J^{-1} F_{il} F_{lL} \kappa_{lL}, \tag{55}$$

$$C_{V}^{"}=I^{-1}C_{V},\tag{56}$$

The symmetrized transformation thermoelastic governing equations and boundary conditions are given by:

$$\left(C''_{ijkl}U''_{l,k} + S''_{ijl}U''_{l} + \beta''_{ij}\Delta T''\right)_{,i} 
\rho''_{ij}\ddot{U}''_{i} + D''_{jkl}U''_{k,l} + E''_{jl}U''_{l} + \gamma''_{j}\Delta T'', \quad \text{in } m', 
\left(\kappa''_{jl}T''_{,l}\right)_{,j} = C''_{V}\dot{T}'' + \beta''_{kl}T_{0}\dot{U}''_{l,k} + \gamma''_{l}T_{0}\dot{U}''_{l}, \quad \text{in } m', 
\eta'_{i}\left(C''_{ijkl}U''_{l,k} + S''_{ijl}U''_{l} + \beta''_{ij}\Delta T''\right)dS\Big|_{\partial m', \text{in}} = \eta_{l}S_{lj}dS\Big|_{\partial M, \text{out}}, 
\eta'_{i}\left(\kappa''_{il}T''_{,l}\right)dS\Big|_{\partial m', \text{in}} = \eta_{l}q_{l}dS\Big|_{\partial M, \text{out}}.$$
(57)

Interestingly, although the displacement field is changed by both gauge matrix and coordinate transformation matrix, the temperature field is only affected by the latter. Therefore, a same temperature distribution with the asymmetric transformation thermoelasticity theory would be obtained under the symmetrized one.

It is worth noting that complete invariance is not exhibited after symmetrization. But form invariance is still retained in the continuity of the normal heat flow, and so is the continuity of tractions under the degradation condition on  $\partial m'$  in Eq. (49). This means that the power flow through boundary  $\partial m'$  is always conserved before and after the transformation. It is to be expected that differences are almost indistinguishable outside m', despite the destruction of the form invariance of the internal governing equations.

Similar to the previous discussion, when the thermoelastic coupling effect is negligible, the above equations will degenerate into a decoupled Willis-type transformation elastic cloak and a decoupled transformation heat cloak:

$$\left(C_{iikl}''U_{l,k}'' + S_{iil}''U_{l}''\right)_{i} = \rho_{ii}''\ddot{U}_{i}'' + D_{ikl}''U_{k,l}'' + E_{il}''U_{l}'', \text{ in } m',$$
 (58)

$$\left(\kappa_{ii}^{"}T_{i}^{"}\right)_{i} = C_{V}^{"}\dot{T}^{"} \quad \text{in } m', \tag{59}$$

with boundary conditions:

$$n'_{i} \left( C''_{ijkl} U''_{l,k} + S''_{ijl} U''_{l} \right) dS \Big|_{\partial m', \text{in}} =$$

$$n_{l} \left( C_{IJKL} U_{L,K} \right) dS \Big|_{\partial M, \text{Out}},$$
(60)

$$n_{j}'(\kappa_{jl}''T_{,l}'')dS\big|_{\partial m',\text{in}} = n_{j}q_{j}dS\big|_{\partial M,\text{out}}.$$
(61)

#### 3. Simulation results

In this section, both transformation thermoelasticity theories described in Sect. II.A and Sect. II.B are explored within the context of an invisibility cloak. For convenience, they are designated as asymmetric and symmetrized dual-function thermoelastic cloaks, respectively. Their performance is evaluated through numerical simulation by comparing with the cases of a uniform medium and of an unprotected hole. The partial differential equation (PDE) package of COMSOL multiphysics is used for numerical calculations in this paper. Due to the continuity condition of Eq. (49) that is introduced by the symmetrization process, the linear affine mapping that is generally considered in the literature is not applicable. Instead, a nonlinear mapping  $\mathcal F$  is adopted. It reads in cylindrical coordinates:

$$r' = \frac{r_1}{r_2^2}r^2 + \frac{r_2 - 2r_1}{r_2}r + r_1, \quad \theta' = \theta, \quad z' = z, \quad r \in M,$$
 (62)

with the monotonicity condition:

$$r_2 \ge 2r_1,\tag{63}$$

where  $r_1$  and  $r_2$  are the inner radius and outer radius of the cloak.  $\mathcal{F}$  satisfies  $r'(r_2) = r_2$ ,  $r'(0) = r_1$ , and  $\mathrm{d}r'/\mathrm{d}r(r_2) = 1$ . Matrix F reads in Cartesian coordinates:

$$F = R(\theta') \begin{bmatrix} dr'/dr & 0 & 0 \\ 0 & r'/r & 0 \\ 0 & 0 & 1 \end{bmatrix} R(-\theta')$$
 (64)

where

$$r(r') = \frac{\sqrt{(r_2 - 2r_1)^2 + 4r_1(r' - r_1)} - (r_2 - 2r_1)}{\frac{2r_1}{r_2}}.$$
 (65)

Consequently, the region  $r' < r_1$  is removed from space  $\Omega$  so that anything placed there would be invisible. One should mention that for a perfect cloak,  $\mathcal{F}(\mathbf{X}=\mathbf{0})$  may not represent a single point in m. However, it will inevitably lead to infinite material parameters, so we replace it with a micropore near the point  $\mathbf{X}=\mathbf{0}$  which would be called as inner-diameter defect in this paper.

Copper is taken as the background medium characterized by lamé constants  $\lambda=95$  GPa and  $\mu=40$  GPa, mass density  $\rho=8960$  kg/m³, isotropic thermal conductivity  $\kappa=397$ W/(m·K), volumetric heat capacity  $C_V=3.5$ J/(m³·K) and isotropic thermal expansion coefficient  $\beta=6$ MPa/K.

## 3.1. Transient elastic wave

High-frequency compressional waves excited by thermalelectro-mechanical coupling are a major problem on microelectronic substrates. Energy transfers between different components in the form of temperature (heat) and mechanical (elastic wave) fluctuations, and finally concentrates at the holes. Thermoelastic energy concentration is one of the main reasons for the reduction of the service life of components and equipments, especially under heavy computational loads. Protective cloaks possibly could reduce this phenomenon.

The numerical model in this section is set as follows. A  $L=20l_0$  long x-polarization line excitation source, located to the left of the cloak a distance  $d=10l_0$  from its center, oscillates at frequency  $f_0=150$ kHz with an amplitude of  $A_0=100~\mu\text{m}$ . The wavelength of the incident longitudinal wave is  $l_0=\sqrt{\lambda+2\mu/\rho}/f_0=29.4$ mm. The inner and outer radius of the cloak is set to  $r_1=l_0$  and  $r_2=3l_0$ , respectively. To ensure convergence, the maximum mesh element size is set to one twentieth of the wavelength  $l_0$ . Transient analysis is performed, since the governing equation for temperature in (3) is a diffusion equation without time-harmonic characteristics. The background boundary is set as both traction-free and thermally insulating. The exact boundary condition has no incidence on the results as long as the background medium is chosen wide enough to avoid reflections. The inner boundary of the cloak is set as traction-free and thermally insulating as well.

The displacement along the *x*-direction shown in Fig. 2 is the primary physical variable under investigation. For reference, Fig. 2(a) shows the unimpeded propagation of thermoelastic waves. Due to the introduction of a hole, as shown in Fig. 2(b), forward propagation of the wave is partially blocked and scattering to the upper and lower sides occurs. Scattering is well removed after covering the hole with the asymmetric dual-function thermoelastic cloak, as shown in Fig. 2(c). The hole is effectively isolated from the background medium by the cloak and has thus little influence on the displacement field. Things are a little different when the symmetrized dual-function thermoelastic cloak covers the hole, as shown in Fig. 2(d). Consistently with the analysis of Sect. II.B, the displacement field outside the cloak region appears visually the same as in Fig. 2(c). However, the displacements inside the cloak

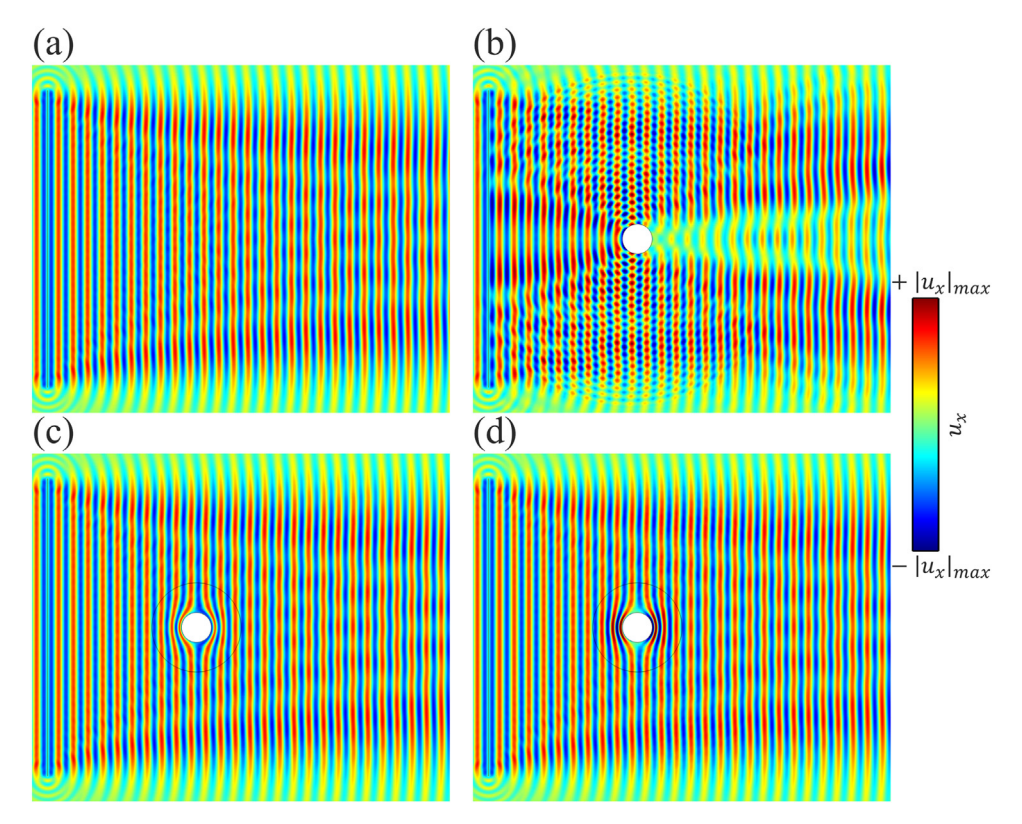


**Fig. 2.** Distribution of displacement  $u_x$  under the excitation of elastic waves in different systems: (a) a homogeneous isotropic medium; (b) the same medium with a traction-free hole; (c) the traction-free hole covered with the asymmetric dual-function thermoelastic cloak; (d) the traction-free hole covered with the symmetrized dual-function thermoelastic cloak.

is significantly rearranged by the gauge matrix. Since Eq. (1) does not define a norm preserving mapping, the amplitude obviously changes. This peculiarity does not affect invisibility but creates some concentration of energy around the hole.

The contrast is more prominent considering the displacement along the y direction, as shown in Fig. 3. Compared with the displacement concentration at the edge of the finite line source, the displacement caused by scattering at the hole in Fig. 3(b) is dominant. The asymmetric dual-function thermoelastic cloak shown in Fig. 3(c) ensures that the external environment is almost unaffected by the hole. The symmetrized cloak shown in Fig. 3(d) also hides the hole in the far field, but some energy concentration occurs in its interior. The difference between both cloaks may be explained from the perspective of the constitutive relations. The asymmetric cloak adopts a constitutive relationship similar to that of chiral materials, see Eqs. (28) and (29). The rotational stiffness is thus the main factor in wave manipulation. In contrast, the symmetrized cloak mainly depends on the unique Willis coupling terms and on the anisotropic mass of Willis materials. As a consequence, waves are redirected by means of the coupling of vibrations along different directions. The difference in the regulation mechanisms may also provide a physical interpretation to the differences in Fig. 2(c)(d). In addition, consistent invisibility of external fields in Figs. 2(c)(d) and Figs. 3(c)(d) is also observed for both regulation mechanisms. This results from the fact that Willis materials share similar characteristics with chiral materials [59], even if coupling is considered. However, for the practical application of symmetrized cloaks based on Willis materials, more attention should be paid to the dramatic increase in internal displacement

Fig. 4 shows the thermal field accompanying high frequency waves, which also implies the transfer of thermal energy on the substrate. The temperature field is mainly dominated by time-

dependent terms in Eq. (3), the volumetric heat capacity in Eqs. (15) and (56), and the thermal expansion tensors in Eqs. (12), (47) and (48). Fig. 4(b) shows the change in the temperature field resulting from the introduction of a hole in the uniform medium. The temperature distribution is obviously affected. Thermal concentration would lead energy to accumulate at the hole over time, which is potentially harmful to the inserts contained in it. Different from the displacement fields, both cloaks (see Fig. 4(c,d)) mask the presence of the hole and guide the heat flow smoothly around it with the same signature. This observation is consistent with the statement that the introduction of the gauge matrix does not affect the temperature field. Furthermore, under the same design strategy, the asymmetric dual-function cloak using chiral materials and the symmetrized cloak using Willis materials always share the same thermal coupling characteristics. The symmetry process is thus not affected by coupling. It can be qualitatively concluded that the features read from these figures are consistent with the discussion in Sect. II.

For quantitative analysis, the disturbance caused by the introduction of the hole and of the cloak must be obtained. Under thermal coupling, the scattered-field formulation may be no longer be applicable. Radiation characteristics are here described by the time-averaged power flow defined by

$$e(\mathbf{r}, t_0) = \frac{1}{T} \int_{t_0}^{t_0+T} -\mathbf{n}(\mathbf{r}) \cdot [\boldsymbol{\sigma}(\mathbf{r}, t) \cdot \dot{\boldsymbol{u}}(\mathbf{r}, t) + \kappa(\mathbf{r}) \cdot \nabla T(\mathbf{r}, t)] dt.$$
(66)

This formula combines both elastic and thermal radiation. Fig. 5 shows power flow from the region  $r < 6l_0$  (abbreviated as  $\psi$ ) as a function of direction, for different configurations. Negative  $e(\mathbf{r}_0, t_0) < 0$  indicates that power flows into  $\psi$  at point  $\mathbf{r}_0$ , whereas positive  $e(\mathbf{r}_0, t_0) > 0$  indicates power radiates from  $\psi$  at point  $\mathbf{r}_0$ .

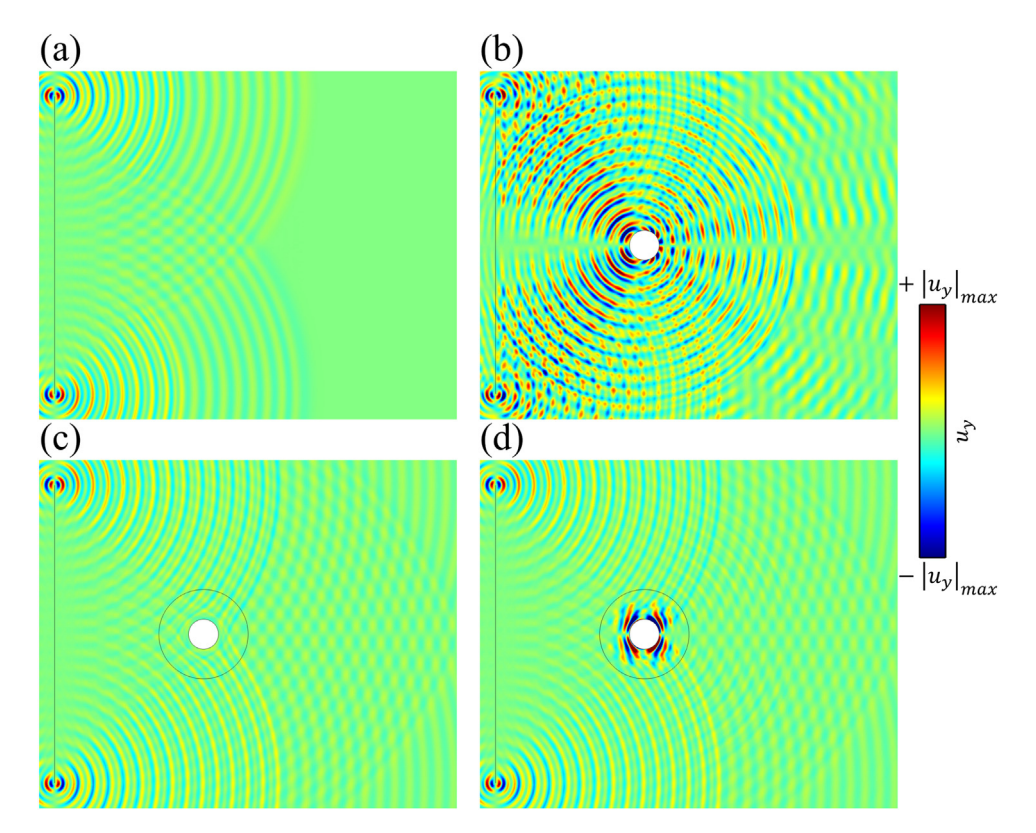


**Fig. 3.** Distribution of displacement  $u_y$  under the excitation of elastic waves in different systems: (a) a homogeneous isotropic medium; (b) the same medium with a traction-free hole; (c) the traction-free hole covered with the asymmetric dual-function thermoelastic cloak; (d) the traction-free hole covered with the symmetrized dual-function thermoelastic cloak.

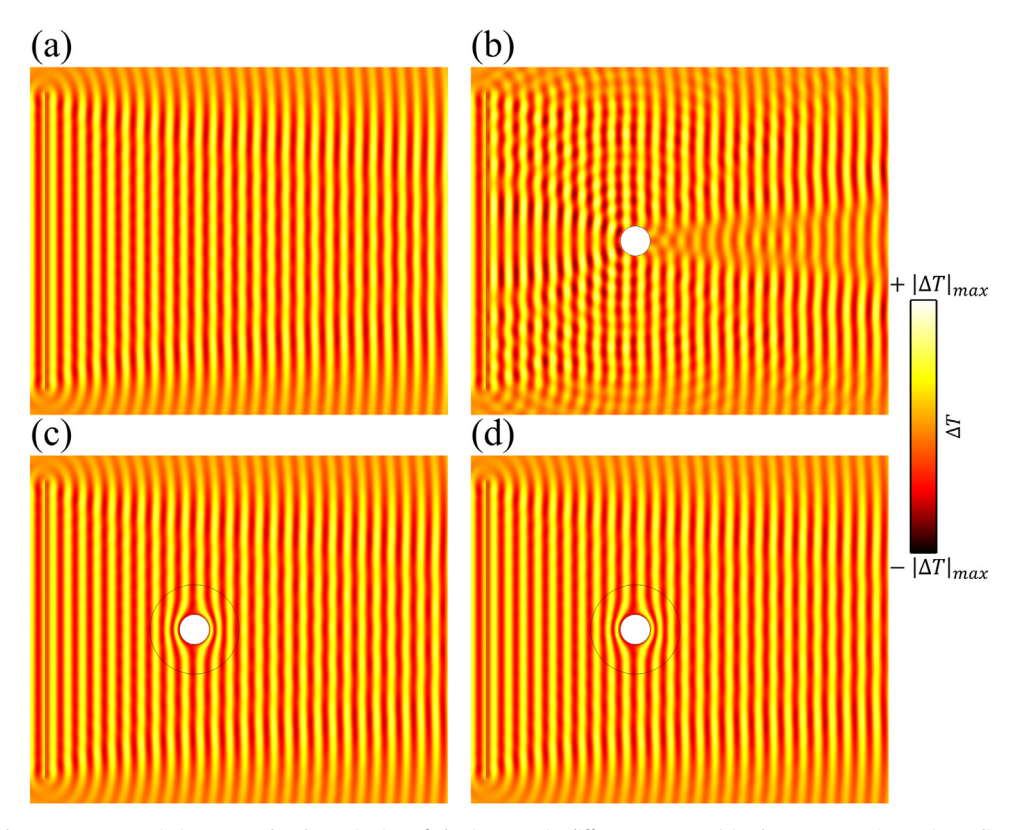


**Fig. 4.** Distribution of the temperature variation  $\Delta T$  under the excitation of elastic waves in different systems: (a) a homogeneous isotropic medium; (b) the same medium with a traction-free hole; (c) the traction-free hole covered with the asymmetric dual-function thermoelastic cloak; (d) the traction-free hole covered with the symmetrized dual-function thermoelastic cloak.

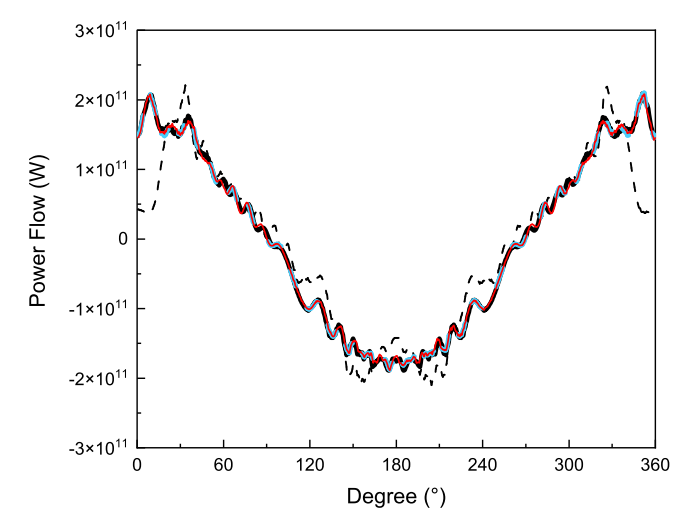


**Fig. 5.** Power flow at distance  $r=6l_0$  as a function of direction. Considered are the homogeneous isotropic medium (black solid curve), the traction-free hole (black dashed curve), the traction-free hole covered with an asymmetric dual-function thermoelastic cloak (blue dashed curve), the traction-free hole covered with a symmetrized dual-function thermoelastic cloak (red solid curve). (For interpretation of the references to colour in this figure legend, the reader is referred to the web version of this article.)

Since the thermoelastic wave is incident from the left, region  $\psi$  always receives power in angles in the range [90°, 270°] and radiates power in other directions. The homogeneous isotropic media

is considered as a reference. After introduction of the hole, scattering from its edge causes a significant change in the power flow characteristics, resulting in a low correlation of 93.15%. Changes are most prominent around  $0^{\circ}$  and in the range  $[90^{\circ}, 270^{\circ}]$ . When the hole is covered with an asymmetric cloak or a symmetrized cloak, the power flow distribution almost coincides with the reference one. The correlation is restored to 99.95% and 99.94%, respectively. Minor deviations, mainly caused by internal diameter defects, can be noticed; though they may be unavoidable they remain inconsequential. In addition, the high coincidence for both cloaks (with a correlation of 99.99%) also shows the practical equivalence of the two transformation thermoelastic theories with regards to radiation.

#### 3.2. Steady heat transfer

The performance of both cloaks is now tested under the application of a temperature gradient applied between the left and right sides of the computation domain. Several existing analyses about cloaking are mostly limited to the temperature field under this operating condition. It is still expected to be extended in the framework of thermoelasticity. The accompanying displacements of the cloaks would be discussed in this section. The numerical model is set as follows. A square with length L is set as the substrate. Its center coincides with the center of the cloak. The inside and outside radiuses of the cloak are identical to Section 3.1. A temperature difference  $\Delta T = 60K$  is applied between the left and the right sides of the substrate. Both upper and lower boundaries, and holes

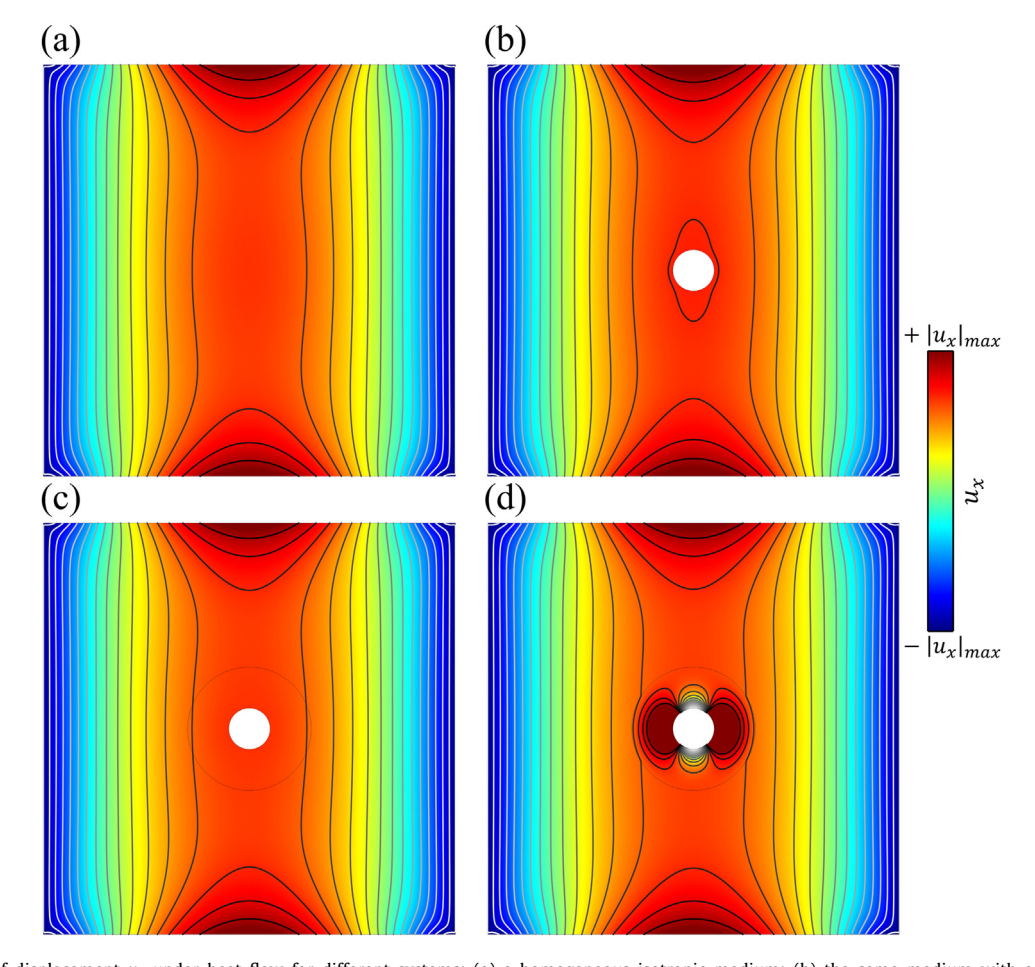


**Fig. 6.** Distribution of displacement  $u_x$  under heat flow for different systems: (a) a homogeneous isotropic medium; (b) the same medium with a traction-free hole; (c) the traction-free hole covered with the asymmetric dual-function thermoelastic cloak; (d) the traction-free hole covered with the symmetrized dual-function thermoelastic cloak.

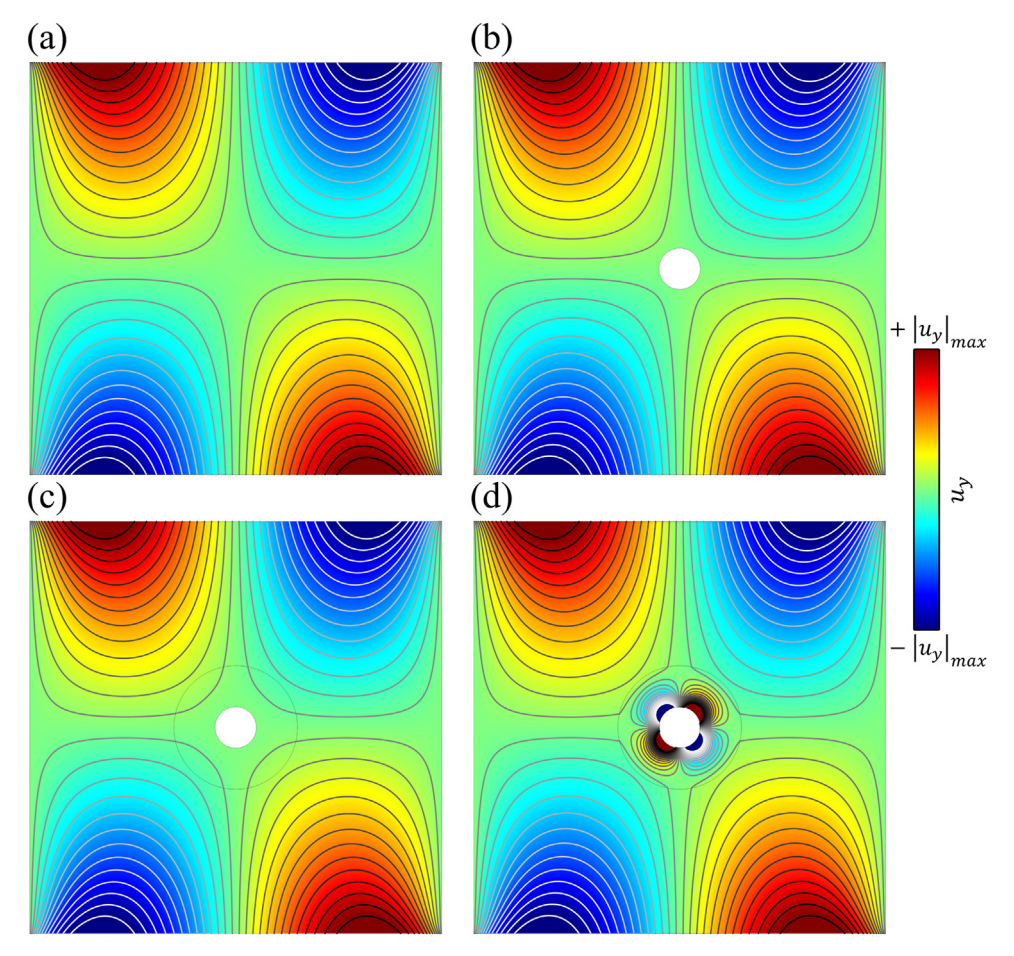


**Fig. 7.** Distribution of displacement  $u_y$  under heat flow for different systems: (a) a homogeneous isotropic medium; (b) the same medium with a traction-free hole; (c) the traction-free hole covered with the symmetrized dual-function thermoelastic cloak; (d) the traction-free hole covered with the symmetrized dual-function thermoelastic cloak;

are set as traction-free and thermally insulating boundaries. Steady state analysis is adopted here.

The displacements  $u_x$  and  $u_y$  caused by the temperature difference are shown in Fig. 6 and Fig. 7. As shown in Fig. 6(a), displacements are enhanced at the free boundaries of the homogeneous substrate. After introduction of the hole, as shown in Fig. 6(b), displacements around the hole increase slightly. The asymmetric cloak shown in Fig. 6(c) counters this increase while leaving the substrate apparently unaffected by the hole. In the case of the symmetrized cloak (Fig. 6(d)), invisibility is still guaranteed. However, the Willis material used in the cloak under steady state shows obvious flexibility, which results in significant displacement variations inside the cloak. Although it has no effect on the background medium, this concentration may lead to compression of inserts placed the hole. Similar features are observed are Fig. 7. The concentration introduced by the symmetrization process is contrary to expectations and may need further improvements. In summary, on the one hand, both dual-function cloaks under heat flow provide invisibility; on the other hand, the symmetrization process may destroy the elastic isolation of the hole from the background media.

The temperature field shown in Fig. 8 is governed only by the steady-state heat conduction equation:

$$\left(\kappa_{IJ}T_{J}\right)_{I}=0. \tag{67}$$

The direction of heat flow in both cloaks is determined by the transformed thermal conductivity (Eq. 13) with the governing

equation:

$$\left(\kappa_{ii}^{\prime}T_{ij}^{\prime}\right)_{i}=0,\tag{68}$$

which is the same as the traditional heat cloak[16]. Obviously, the temperature field is decoupled in the steady state. Therefore, relevant conclusions are consistent with the previous literature on the heat cloak.

#### 4. Discussion and conclusion

In this paper, transformation theory has been extended to the framework of thermoelasticity. The governing equations for transformation thermoelasticy are derived. Two transformation theories, involving either asymmetric or symmetrized elastic tensors, are given. The retention and absence of form invariance in the governing equations and flux conditions are analyzed. A degradation condition is induced in the symmetrization process, which can be met by a properly designed nonlinear mapping. Numerical simulations are conducted on two operation conditions within the context of a dual-function transformation thermoelastic invisibility cloak.

Under transient elastic wave excitation, cloaks designed by both theories ensure invisibility and isolation of the hole from the outside field. The uniformity of the two transformation thermoelasticity theories has been verified. Very similar temperature fields are observed for both theories under the same mapping  $\mathcal{F}$ . Mathematical and physical interpretations are given for the differences in the

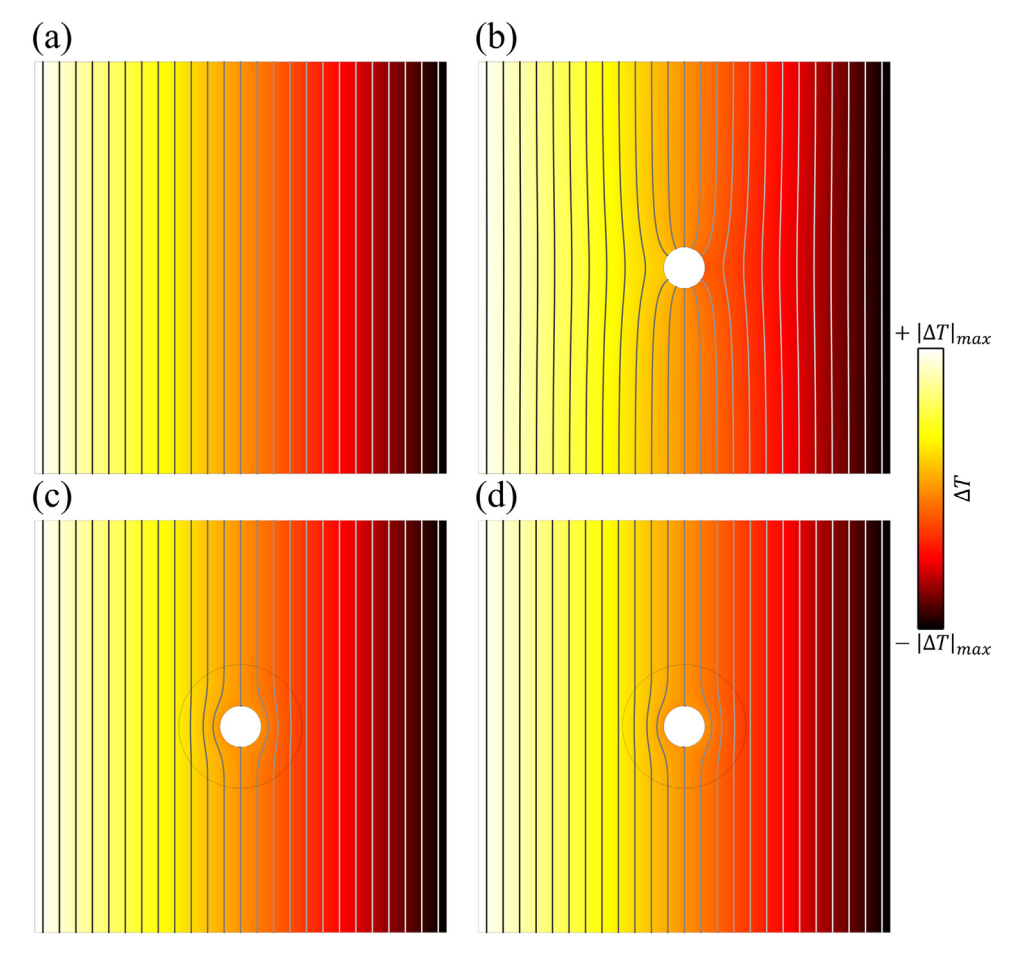


**Fig. 8.** Distribution of the temperature variation  $\Delta T$  under heat flow for different systems: (a) a homogeneous isotropic medium; (b) the same medium with a traction-free hole; (c) the traction-free hole covered with the asymmetrized dual-function thermoelastic cloak; (d) the traction-free hole covered with the symmetrized dual-function thermoelastic cloak.

displacement fields resulting from the symmetrization process. A time-averaged power flow is proposed to verify quantitatively the performance of the cloaks. The uniformity of the two transformation thermoelasticity theories has been verified.

Under steady heat transfer, it is still found that invisibility is maintained for both displacement and temperature fields. However, the Willis material used in the symmetrized cloak shows obviously large displacements around the hole. This softness may result in compression of inserts in the hole.

Our work attempts to advance transformation theory to multiphysical processes. The regulation of heat flow and elastic waves is further extended from the perspective of thermoelasticity. It is expected that the relevant conclusions can provide a basis for the design of protective equipment. It is still worth noting that the asymmetric thermal expansion tensor and the newly introduced physical quantities resulting from symmetrization still need further exploration. In addition, the dramatic increase and the singularity of material parameters at the inner radius of the cloak also requires a remedy. From the perspective of transformation thermoelasticity, the symmetrized cloak appears to be valuable, owing to the fact that the terms  $S_{ijl}''U_l'''$  and  $D_{jkl}''U_{k,l}''$  are in similar positions with  $\beta_{ij}''\Delta T''$  and  $\gamma_j''\Delta T'''$  in the first formula of Eq. (57). If their contributions could be minimized or even made to cancel each other through optimization, it would be convenient. More detailed design of practical cloaks may be achieved with the help of effective medium theory and experimental verification, which remains to be carried out in the future.

# **Declaration of Competing Interest**

The authors declare that they have no known competing financial interests or personal relationships that could have appeared to influence the work reported in this paper.

# **CRediT authorship contribution statement**

**Yu-Ze Tian:** Methodology, Software, Writing – original draft. **Yan-Feng Wang:** Supervision, Formal analysis, Writing – review & editing. **Gan-Yun Huang:** Supervision, Conceptualization, Writing – review & editing. **Vincent Laude:** Validation, Writing – review & editing. **Yue-Sheng Wang:** Writing – review & editing.

#### Acknowledgments

The authors acknowledge financial support by the National Natural Science Foundation of China (12122207, 12021002, 12192212 and 11991032). Y.F.W. acknowledges support by the Natural Science Foundation of Tianjin, China (20JCQNJC01030). V.L. acknowledges financial support by the EIPHI Graduate School (ANR-17-EURE-0002).

#### References

[1] Y.-F. Wang, Y.-Z. Wang, B. Wu, W. Chen, Y.-S. Wang, Tunable and active phononic crystals and metamaterials, Appl. Mech. Rev. 72 (2020) 040801.

- [2] X. Ni, Z.J. Wong, M. Mrejen, Y. Wang, X. Zhang, An ultrathin invisibility skin cloak for visible light, Science 349 (6254) (2015) 1310–1314.
- [3] Y.R. Padooru, A.B. Yakovlev, P.-Y. Chen, A. Alu, Analytical modeling of conformal mantle cloaks for cylindrical objects using sub-wavelength printed and slotted arrays, J. Appl. Phys. 112 (3) (2012) 034907.
- [4] D. Rainwater, A. Kerkhoff, K. Melin, J. Soric, G. Moreno, A. Alù, Experimental verification of three-dimensional plasmonic cloaking in free-space, New J. Phys. 14 (1) (2012) 013054.
- [5] A. Greenleaf, M. Lassas, G. Uhlmann, On nonuniqueness for calderon's inverse problem, Math. Res. Lett. 10 (5) (2003).
- [6] J.B. Pendry, D. Schurig, D.R. Smith, Controlling electromagnetic fields, Science 312 (5781) (2006) 1780–1782.
- [7] U. Leonhardt, Optical conformal mapping, Science 312 (5781) (2006) 1777–1780.
- [8] S.A. Cummer, D. Schurig, One path to acoustic cloaking, New J. Phys. 9 (3) (2007) 45.
- [9] H. Chen, C. Chan, Acoustic cloaking in three dimensions using acoustic metamaterials, Appl. Phys. Lett. 91 (18) (2007) 183518.
- [10] M. Farhat, S. Guenneau, S. Enoch, A.B. Movchan, Cloaking bending waves propagating in thin elastic plates, Phys. Rev. B 79 (3) (2009) 033102.
- [11] A. Zareei, M.-R. Alam, Broadband cloaking of flexural waves, Phys. Rev. E 95 (6) (2017) 063002.
- [12] A. Golgoon, A. Yavari, Transformation cloaking in elastic plates, Journal of Nonlinear Science 31 (1) (2021) 1–76.
- [13] D. Schurig, J.J. Mock, B. Justice, S.A. Cummer, J.B. Pendry, A.F. Starr, D.R. Smith, Metamaterial electromagnetic cloak at microwave frequencies, Science 314 (5801) (2006) 977–980.
- [14] B.-I. Popa, L. Zigoneanu, S.A. Cummer, Experimental acoustic ground cloak in air, Phys. Rev. Lett. 106 (25) (2011) 253901.
- [15] A. Darabi, A. Zareei, M.-R. Alam, M.J. Leamy, Experimental demonstration of an ultrabroadband nonlinear cloak for flexural waves, Phys. Rev. Lett. 121 (17) (2018) 174301.
- [16] C. Fan, Y. Gao, J. Huang, Shaped graded materials with an apparent negative thermal conductivity, Appl. Phys. Lett. 92 (25) (2008) 251907.
- [17] S. Guenneau, T. Puvirajesinghe, Fick'S second law transformed: one path to cloaking in mass diffusion, J. Roy. Soc. Interface 10 (83) (2013) 20130106.
- [18] M. Farhat, S. Enoch, S. Guenneau, A. Movchan, Broadband cylindrical acoustic cloak for linear surface waves in a fluid, Phys. Rev. Lett. 101 (13) (2008) 134501.
- [19] S. Zhang, D.A. Genov, C. Sun, X. Zhang, Cloaking of matter waves, Phys. Rev. Lett. 100 (12) (2008) 123002.
- [20] G.W. Milton, M. Briane, J.R. Willis, On cloaking for elasticity and physical equations with a transformation invariant form, New J. Phys. 8 (10) (2006) 248.
- [21] J.R. Willis, Variational principles for dynamic problems for inhomogeneous elastic media, Wave Motion 3 (1) (1981) 1–11.
- [22] M. Brun, S. Guenneau, A.B. Movchan, Achieving control of in-plane elastic waves, Appl. Phys. Lett. 94 (6) (2009) 061903.
- [23] H. Nassar, Y. Chen, G. Huang, A degenerate polar lattice for cloaking in full two-dimensional elastodynamics and statics, Proceedings of the Royal Society A 474 (2219) (2018) 20180523.
- [24] X. Xu, C. Wang, W. Shou, Z. Du, Y. Chen, B. Li, W. Matusik, N. Hussein, G. Huang, Physical realization of elastic cloaking with a polar material, Phys. Rev. Lett. 124 (11) (2020) 114301.
- [25] A.N. Norris, A.L. Shuvalov, Elastic cloaking theory, Wave Motion 48 (6) (2011) 525–538.
- [26] A.N. Norris, Acoustic cloaking theory, Proceed. Roy. Soc. A 464 (2097) (2008) 2411–2434
- [27] L. He, L. Cai, X. Chen, Pentamode-based coding metasurface for underwater acoustic stealth, J. Appl. Math. Phys. 9 (7) (2021) 1829–1836.
- [28] Y. Gu, H. Long, Y. Cheng, M. Deng, X. Liu, Ultrathin composite metasurface for absorbing subkilohertz low-frequency underwater sound, Phys. Rev. Appl, 16 (1) (2021) 014021.
- [29] Z. Sun, Y. Shi, X. Sun, H. Jia, Z. Jin, K. Deng, J. Yang, Underwater acoustic multiplexing communication by pentamode metasurface, J, Phys, D Appl, Phys, 54 (20) (2021) 205303.
- [30] S.-J. Joo, B. Park, D.-H. Kim, D.-O. Kwak, J. Park, H.-S. Kim, Bi-directional homogenization equivalent modeling for the prediction of thermo-mechanical properties of a multi-layered printed circuit board (pcb), J. Micromech. Microeng. 26 (4) (2016) 045006.
- [31] M. Nagaraj, C.S. Suh, On short-time-scale stress wave phenomena and initiation of mechanical faults in flip-chip configurations, IEEE Trans. Device Mater. Reliab. 5 (2) (2005) 224–230.
- [32] S. Arakelyan, H. Lee, Y. Jeong, A. Babajanyan, B. Friedman, K. Lee, Direct imaging of the ssd and usb memory drives heating by thermo-elastic optical indicator microscopy, Case Stud. Therm. Eng. 10 (2017) 407–412.

- [33] H. Lee, S. Arakelyan, B. Friedman, K. Lee, Temperature and microwave near field imaging by thermo-elastic optical indicator microscopy, Sci Rep 6 (1) (2016) 1–11.
- [34] X. Qi, C.S. Suh, Generalized thermo-elastodynamics for semiconductor material subject to ultrafast laser heating. part i: model description and validation, Int. I. Heat Mass Transf. 53 (1–3) (2010) 41–47.
- [35] X. Qi, C.S. Suh, Generalized thermo-elastodynamics for semiconductor material subject to ultrafast laser heating, part ii: near-field response and damage evaluation, Int. J. Heat Mass Transf. 53 (4) (2010) 744–752.
- [36] F. Syvret, D. Al-Attar, Thermoelastic cloaking and the breaking of invisibility, arXiv preprint arXiv:1903.06664 (2019).
- [37] Y. Zhou, J. Chen, L. Liu, Z. Fan, Y. Ma, Magnetic-acoustic biphysical invisible coats for underwater objects, NPG Asia Mater. 12 (1) (2020) 1–11.
- [38] J. Zhan, Y. Mei, K. Li, Y. Zhou, J. Chen, Y. Ma, Conformal metamaterial coats for underwater magnetic-acoustic bi-invisibility, Appl Phys Lett 120 (9) (2022) 094104.
- [39] G. Fujii, Y. Akimoto, Electromagnetic-acoustic biphysical cloak designed through topology optimization, Opt. Express 30 (4) (2022) 6090–6106.
- [40] J. Li, Y. Gao, J. Huang, A bifunctional cloak using transformation media, J. Appl. Phys. 108 (7) (2010) 074504.
- [41] Y. Ma, Y. Liu, M. Raza, Y. Wang, S. He, Experimental demonstration of a multiphysics cloak: manipulating heat flux and electric current simultaneously, Phys. Rev. Lett. 113 (20) (2014) 205501.
- [42] T. Stedman, L.M. Woods, Cloaking of thermoelectric transport, Sci. Rep. 7 (1) (2017) 1–8.
- [43] J.C.Á. Hostos, V.D. Fachinotti, I. Peralta, Metamaterial for elastostatic cloaking under thermal gradients, Sci. Rep. 9 (1) (2019) 1–9.
- [44] M.A. Biot, Thermoelasticity and irreversible thermodynamics, J. Appl. Phys. 27 (3) (1956) 240–253.
- [45] C.S. Ha, E. Hestekin, J. Li, M.E. Plesha, R.S. Lakes, Controllable thermal expansion of large magnitude in chiral negative poisson's ratio lattices, Physica Status Solidi (b) 252 (7) (2015) 1431–1434.
- [46] A.C. Eringen, Microcontinuum Field Theories: I. foundations and solids, Springer Science and Business Media, 2012.
- [47] I. Fernandez-Corbaton, C. Rockstuhl, P. Ziemke, P. Gumbsch, A. Albiez, R. Schwaiger, T. Frenzel, M. Kadic, M. Wegener, New twists of 3d chiral metamaterials, Adv. Mater. 31 (26) (2019) 1807742.
- [48] H. Chen, C.T. Chan, Acoustic cloaking and transformation acoustics, J. Phys. D Appl. Phys. 43 (11) (2010) 113001.
- [49] B. Ling, K. Wei, Z. Qu, D. Fang, Design and analysis for large magnitudes of programmable poisson's ratio in a series of lightweight cylindrical metastructures, Int. J. Mech. Sci. 195 (2021) 106220.
- [50] B. Ling, K. Wei, Z. Wang, X. Yang, Z. Qu, D. Fang, Experimentally program large magnitude of Poisson's ratio in additively manufactured mechanical metamaterials, Int. J. Mech. Sci. 173 (2020) 105466.
- [51] X. Chen, N. Laforge, Q. Ji, H. Tan, J. Liang, G. Ulliac, J. Moughames, S. Adrar, V. Laude, M. Kadic, Introduction to mechanical metamaterials and their effective properties, C R Phys. 21 (7–8) (2020) 751–765.
- [52] G.W. Milton, A.V. Cherkaev, Which elasticity tensors are realizable? J. Eng. Mater. Technol. (1995).
- [53] G. Yi, B.D. Youn, A comprehensive survey on topology optimization of phononic crystals, Struct. Multidiscip. Optim. 54 (5) (2016) 1315–1344.
- [54] C.B. Dilgen, S.B. Dilgen, N. Aage, J.S. Jensen, Topology optimization of acoustic mechanical interaction problems: a comparative review, Struct. Multidiscip. Optim. 60 (2) (2019) 779–801.
- [55] W. Li, F. Meng, Y. Chen, Y.f. Li, X. Huang, Topology optimization of photonic and phononic crystals and metamaterials: a review, Adv. Theory Simul. 2 (7) (2019) 1900017.
- [56] X. Ni, X. Guo, J. Li, Y. Huang, Y. Zhang, J.A. Rogers, 2D mechanical metamaterials with widely tunable unusual modes of thermal expansion, Adv. Mater. 31 (48) (2019) 1905405.
- [57] K. Wei, X. Xiao, J. Chen, Y. Wu, M. Li, Z. Wang, Additively manufactured bimaterial metamaterial to program a wide range of thermal expansion, Mater. Des. 198 (2021) 109343.
- [58] X. Guo, X. Ni, J. Li, H. Zhang, F. Zhang, H. Yu, J. Wu, Y. Bai, H. Lei, Y. Huang, et al., Designing mechanical metamaterials with kirigami-inspired, hierarchical constructions for giant positive and negative thermal expansion, Adv. Mater. 33 (3) (2021) 2004919.
- [59] M. Kadic, A. Diatta, T. Frenzel, S. Guenneau, M. Wegener, Static chiral willis continuum mechanics for three-dimensional chiral mechanical metamaterials, Phys. Rev. B 99 (21) (2019) 214101.
- [60] G. Fujii, Y. Akimoto, Optimizing the structural topology of bifunctional invisible cloak manipulating heat flux and direct current, Appl Phys Lett 17 (115) (2019) 174101.